

Chromatic Framework for Vision in Bad Weather*

Srinivasa G. Narasimhan and Shree K. Nayar

Department of Computer Science, Columbia University
New York, New York 10027

Email: {srinivas, nayar}@cs.columbia.edu

Abstract

Conventional vision systems are designed to perform in clear weather. However, any outdoor vision system is incomplete without mechanisms that guarantee satisfactory performance under poor weather conditions. It is known that the atmosphere can significantly alter light energy reaching an observer. Therefore, atmospheric scattering models must be used to make vision systems robust in bad weather. In this paper, we develop a geometric framework for analyzing the chromatic effects of atmospheric scattering. First, we study a simple color model for atmospheric scattering and verify it for fog and haze. Then, based on the physics of scattering, we derive several geometric constraints on scene color changes, caused by varying atmospheric conditions. Finally, using these constraints we develop algorithms for computing fog or haze color, depth segmentation, extracting three dimensional structure, and recovering “true” scene colors, from two or more images taken under different but unknown weather conditions.

1 Vision and Bad Weather

Current vision algorithms assume that the radiance from a scene point reaches the observer unaltered. However, it is well known from atmospheric physics that the atmosphere scatters light energy radiating from scene points. Ultimately, vision systems must deal with realistic atmospheric conditions to be effective outdoors. Several models describing the visual manifestations of the atmosphere can be found in atmospheric optics (see [Mid52], [McC75]). These models can be exploited to not only remove bad weather effects, but also to recover valuable scene information.

Surprisingly, little work has been done in computer vision on weather related issues. Cozman and Krotkov[CK97] computed depth cues from iso-intensity points. Nayar and Narasimhan[NN99] used well established atmospheric scattering models, namely, attenuation and airlight, to extract complete scene structure from one or two images, irre-

spective of scene radiances. They also proposed a *dichromatic* atmospheric scattering model that describes the dependence of atmospheric scattering on wavelength. However, the algorithm they developed to recover structure using this model, requires a clear day image of the scene.

In this paper, we develop a general chromatic framework for the analysis of images taken under poor weather conditions. The wide spectrum of atmospheric particles makes a general study of vision in bad weather hard. So, we limit ourselves to weather conditions that result from fog and haze. We begin by describing the key mechanisms of scattering. Next, we analyze the dichromatic model proposed in [NN99], and experimentally verify it for fog and haze. Then, we derive several useful geometric constraints on scene color changes due to different but *unknown* atmospheric conditions. Finally, we develop algorithms to compute fog or haze color, to construct depth maps of arbitrary scenes, and to recover scene colors as they would appear on a clear day. All of our methods only require images of the scene taken under two or more *poor* weather conditions, and not a clear day image of the scene.

2 Mechanisms of Scattering

The interactions of light with the atmosphere can be broadly classified into three categories, namely, scattering, absorption and emission. Of these, scattering due to suspended atmospheric particles is most pertinent to us. For a detailed treatment of the scattering patterns and their relationship to particle shapes and sizes, we refer the reader to the works of [Mid52] and [Hul57]. Here, we focus on the two fundamental scattering phenomena, namely, airlight and attenuation, which form the basis of our framework.

2.1 Airlight

While observing an extensive landscape, we quickly notice that the scene points appear progressively lighter as our attention shifts from the foreground toward the horizon. This phenomenon, known as *airlight* (see [Kos24]), results from the scattering of environmental light toward the observer, by the atmospheric particles within the observer’s cone of vision.

*This work was supported in parts by a DARPA/ONR MURI Grant(N00014-95-1-0601), an NSF National Young Investigator Award, and a David and Lucile Packard Fellowship.

The radiance of airlight increases with pathlength d and is given by (see [McC75] and [NN99]),

$$L(d, \lambda) = L_\infty(\lambda)(1 - e^{-\beta(\lambda)d}). \quad (1)$$

$\beta(\lambda)$ is called the total scattering coefficient and it represents the ability of a volume to scatter flux of a given wavelength λ , in all directions. $\beta(\lambda)d$ is called the optical thickness for the pathlength d . $L_\infty(\lambda)$ is known as the ‘‘horizon’’ radiance. More precisely, it is the radiance of the airlight for an infinite pathlength. As expected, the airlight at the observer ($d = 0$) is zero.

Assuming a camera with a linear radiometric response, the image irradiance due to airlight can be written as $E(d, \lambda) = gL_\infty(\lambda)(1 - e^{-\beta(\lambda)d})$, where g accounts for the camera parameters. Substituting

$$E_\infty(\lambda) = gL_\infty(\lambda), \quad (2)$$

we obtain

$$E(d, \lambda) = E_\infty(\lambda)(1 - e^{-\beta(\lambda)d}). \quad (3)$$

2.2 Attenuation

As a light beam travels from a scene point through the atmosphere, it gets attenuated due to scattering by atmospheric particles. The attenuated flux that reaches an observer from a scene point, is termed as *direct transmission* [McC75]. The direct transmission for collimated light beams is given by Bouguer’s exponential law[Bou30]:

$$E(d, \lambda) = g L_0(\lambda)e^{-\beta(\lambda)d}, \quad (4)$$

where $E(d, \lambda)$ is the attenuated irradiance at the observer, and $L_0(\lambda)$ is the radiance of the scene point prior to attenuation. Again, g accounts for the camera parameters. Allard’s law[All76] modifies the above model for divergent light beams from point sources as

$$E(d, \lambda) = g \frac{I_0(\lambda)e^{-\beta(\lambda)d}}{d^2}, \quad (5)$$

where $I_0(\lambda)$ is the radiant intensity of the point source. In the subsequent sections, we use the terms ‘‘attenuation model’’ and ‘‘direct transmission model’’, interchangeably.

2.3 Overcast Sky Illumination

Allard’s attenuation model is in terms of the radiant intensity of a *point source*. This formulation does not take into account the sky illumination and its reflection by scene points. We make two simplifying assumptions regarding the illumination received by a scene point. Then, we reformulate the attenuation model in terms of sky illumination and the BRDF of scene points.

Usually, the sky is overcast under foggy conditions. So we use the overcast sky model for environmental illumination[GC66][MS42]. We also assume that the irradiance at each scene point is dominated by the radiance of the sky, and that the irradiance due to other scene points is not significant. In Appendix A, we have shown that the attenuated irradiance at the observer is given by,

$$E(d, \lambda) = g \frac{L_\infty(\lambda) r e^{-\beta(\lambda)d}}{d^2}. \quad (6)$$

where $L_\infty(\lambda)$ is the horizon radiance. r represents the sky aperture (the cone of sky visible from a scene point), and the reflectance of the scene point in the direction of the viewer. From (2), we have

$$E(d, \lambda) = \frac{E_\infty(\lambda) r e^{-\beta(\lambda)d}}{d^2}. \quad (7)$$

The above expression for the direct transmission of a scene point includes the effects of sky illumination and the reflectance of the scene point. In the remainder of the paper, we refer to (7) as the direct transmission model.

3 Dichromatic Model

Hitherto, we have described attenuation and airlight separately. At *night*, there can be no airlight (since there is no environmental illumination) and hence, attenuation dominates. In contrast, under *dense* fog or haze during daylight, the radiance from a scene point is severely attenuated and hence airlight dominates. However, in most situations the effects of both attenuation and airlight coexist. Here, we discuss the chromatic effects of atmospheric scattering that include both attenuation and airlight.

Nayar and Narasimhan[NN99] derived a color model for atmospheric scattering called the dichromatic atmospheric scattering model. It states that the color of a scene point under bad weather is a linear combination of the direct transmission color (as seen on a clear day, when there is minimal atmospheric scattering), and airlight color (fog or haze color).

Figure 1 illustrates the dichromatic model in R-G-B color space. Let \mathbf{E} be the observed color vector for a scene point P , on a foggy or hazy day. Let the unit vector $\hat{\mathbf{D}}$ represent the direction of direct transmission color of P . Let the unit vector $\hat{\mathbf{A}}$ represent the direction of airlight color. Then, we can write

$$\mathbf{E} = p \hat{\mathbf{D}} + q \hat{\mathbf{A}}, \quad (8)$$

where p is the magnitude of direct transmission, and q is the magnitude of airlight of P .

For the visible light spectrum, the relationship between the scattering coefficient β , and the wavelength λ , is given by

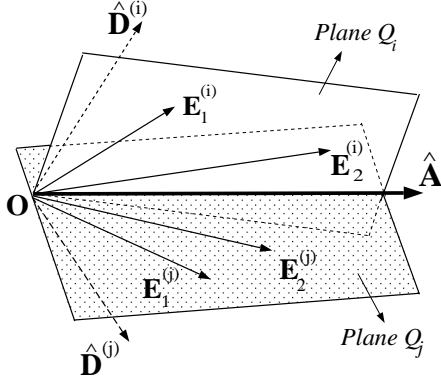


Figure 3: Intersection of two different dichromatic planes yields the direction $\hat{\mathbf{A}}$ of airlight color.

In practice, scenes have several points with different colors. Therefore, we can compute a robust intersection of several dichromatic planes by minimizing the objective function

$$\epsilon = \sum_i (\mathbf{N}_i \cdot \hat{\mathbf{A}})^2. \quad (13)$$

Thus, we are able to compute the color of fog or haze using only the observed colors of the scene points under two atmospheric conditions, and not relying on a patch of the sky being visible in the image.

We verified the above method for the two scenes shown in figures 6(a) and (c). First, the direction of airlight color was computed using (13). Then, we compared it with the direction of the airlight color obtained by averaging an unsaturated patch of the sky. For the two scenes, the angular deviations were found to be 1.2° and 1.6° respectively. These small errors in the computed directions of airlight color indicate the robustness of the method.

5 Iso-depth Scene Points

In this section, we derive a simple constraint for scene points that are at the same depth from the observer. This constraint can then be used to segment the scene based on depth, *without* knowing the actual reflectances of the scene points and their sky apertures. For this, we first prove the following lemma.

Lemma 1 *Ratios of the direct transmission magnitudes for points under two different weather conditions are equal, if and only if the scene points are at equal depths from the observer.*

Proof: Let β_1 and β_2 be two unknown weather conditions with horizon brightness values E_{∞_1} and E_{∞_2} . Let P_i and P_j be two scene points at depths d_i and d_j , from the observer. Also, let $r^{(i)}$ and $r^{(j)}$ represent sky apertures and reflectances of these points.

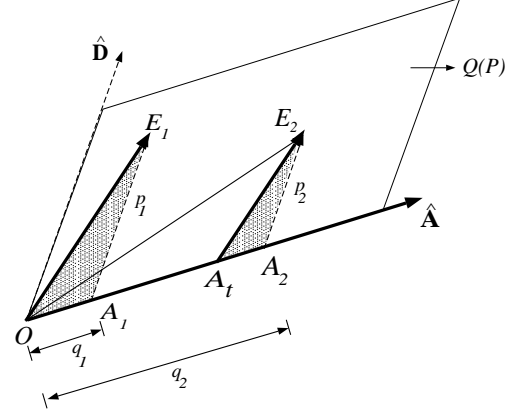


Figure 4: The ratio p_2 / p_1 of the direct transmissions for a scene point under two different atmospheric conditions is equal to the ratio $|E_2 A_t| / |E_1 O|$ of the parallel sides. Shaded triangles are similar.

From (10), the direct transmission magnitudes of P_i under β_1 and β_2 , can be written as

$$\begin{aligned} p_1^{(i)} &= \frac{E_{\infty_1} r^{(i)} e^{-\beta_1 d_i}}{d_i^2}, \\ p_2^{(i)} &= \frac{E_{\infty_2} r^{(i)} e^{-\beta_2 d_i}}{d_i^2}. \end{aligned} \quad (14)$$

Similarly, the direct transmission magnitudes of P_j under β_1 and β_2 , are

$$\begin{aligned} p_1^{(j)} &= \frac{E_{\infty_1} r^{(j)} e^{-\beta_1 d_j}}{d_j^2}, \\ p_2^{(j)} &= \frac{E_{\infty_2} r^{(j)} e^{-\beta_2 d_j}}{d_j^2}. \end{aligned} \quad (15)$$

Then, we immediately see that the relation:

$$\frac{p_2^{(i)}}{p_1^{(i)}} = \frac{p_2^{(j)}}{p_1^{(j)}} = \left(\frac{E_{\infty_2}}{E_{\infty_1}} \right) e^{-(\beta_2 - \beta_1)d}, \quad (16)$$

holds if and only if $d_i = d_j = d$. So, if we have the ratio of direct transmissions for each pixel in the image, we can group the scene points according to their depths from the observer. But how do we compute this ratio for any scene point without knowing the actual direct transmission magnitudes?

Consider the dichromatic plane geometry for a scene point P , as shown in figure (4). Here, we denote a vector by the line segment between its end points. Let p_1 and p_2 be the unknown direct transmission magnitudes of P under β_1 and β_2 , respectively. Similarly, let q_1 and q_2 be the unknown airlight magnitudes for P under β_1 and β_2 .

We define an airlight magnitude $|OA_t|$ such that

$$\overline{E_2 A_t} \parallel \overline{E_1 O}. \quad (17)$$

Also, since the *direction* of direct transmission color for a scene point does not vary due to different atmospheric conditions, $\overline{E_1 A_1} \parallel \overline{E_2 A_2}$. Here A_1 and A_2 correspond to the end points of the airlight magnitudes of P under β_1 and β_2 , as shown in figure (4). Thus, $\triangle E_1 O A_1 \sim \triangle E_2 A_t A_2$. This implies,

$$\frac{p_2}{p_1} = \frac{q_2 - |O A_t|}{q_1} = \frac{|E_2 A_t|}{|E_1 O|}. \quad (18)$$

Since the right hand side of (18) can be computed using the observed color vectors of the scene point P , we can compute the ratio (p_2 / p_1) of direct transmission magnitudes for P under two atmospheric conditions. Therefore, from (16), we have a simple method to find points at the same depth, *without* having to know their reflectances and sky apertures. A sequential labeling like algorithm can then be used to efficiently segment scenes into regions of equal depth.

6 Scene structure

We extend the direct transmission ratio constraint given in (16) one step further and present a method to construct the complete structure of an arbitrary scene, from two images taken under poor weather conditions.

From (16), the ratio of direct transmissions of a scene point P under two atmospheric conditions, is given by

$$\frac{p_2}{p_1} = \frac{E_{\infty_2}}{E_{\infty_1}} e^{-(\beta_2 - \beta_1)d}. \quad (19)$$

Note that we have already computed the left hand side of the above equation using (18). Taking natural logarithms on both sides, we get

$$(\beta_2 - \beta_1)d = \ln \left(\frac{E_{\infty_2}}{E_{\infty_1}} \right) - \ln \left(\frac{p_2}{p_1} \right). \quad (20)$$

So, if we know the horizon brightness values, E_{∞_1} and E_{∞_2} , then we can compute the scaled depth $(\beta_2 - \beta_1)d$ at P . In fact, $(\beta_2 - \beta_1)d$ is the Difference in Optical Thicknesses (DOT) for the pathlength d , under the two weather conditions. In the atmospheric optics literature, the term DOT is used as a quantitative measure of the “change” in weather conditions.

6.1 Estimation of E_{∞_1} and E_{∞_2}

The expression for scaled depth given in (20), includes the horizon brightness values, E_{∞_1} and E_{∞_2} . These two terms are *observables* only if some part of the sky is visible in the image. However, the brightness values within the region of the image corresponding to the sky, cannot be trusted since they are prone to intensity saturation and color clipping. Here, we estimate E_{∞_1} and E_{∞_2} using only points in the “non-sky” region of the scene.

Let q_1 and q_2 denote the magnitudes of airlight for a scene point P under atmospheric conditions β_1 and β_2 . Using (10), we have

$$\begin{aligned} q_1 &= E_{\infty_1} (1 - e^{-\beta_1 d}), \\ q_2 &= E_{\infty_2} (1 - e^{-\beta_2 d}). \end{aligned} \quad (21)$$

Therefore,

$$\frac{E_{\infty_2} - q_2}{E_{\infty_1} - q_1} = \frac{E_{\infty_2}}{E_{\infty_1}} e^{-(\beta_2 - \beta_1)d}. \quad (22)$$

Substituting (19), we can rewrite the above equation as

$$\left(\frac{p_2}{p_1} \right) = \frac{q_2 - c}{q_1}, \quad (23)$$

where,

$$c = E_{\infty_2} - \left(\frac{p_2}{p_1} \right) E_{\infty_1}. \quad (24)$$

Comparing (23) and (18), we get $c = |O A_t|$ (see figure (4)). Hence, (24) represents a straight line equation in the unknown parameters, E_{∞_1} and E_{∞_2} .

Now consider several pairs of $\{c^{(i)}, (p_2^{(i)} / p_1^{(i)})\}$ corresponding to scene points P_i , at different depths. Then, the estimation of E_{∞_1} and E_{∞_2} is reduced to a *line fitting* problem. Quite simply, we have shown that the horizon brightnesses under different weather conditions can be computed using *only* non-sky scene points.

Since both the terms on the right hand side of (20) can be computed for every scene point, we have a simple algorithm for computing the scaled depth at each scene point, and hence the complete scene structure, from two bad weather images.

6.2 Experimental Results

We now present results showing scene structure recovered from both synthetic and real images. The synthetic scene we used is shown on the left side of figure 5(a) as a 200×200 pixel image with 16 color patches. The colors in this image represent the direct transmission or “true” colors of the scene. We assigned a random depth value to each color patch. The rotated 3D structure of the scene is shown on the right side of figure 5(a). Then, two different levels of fog ($\beta_1 = 1.0$, $\beta_2 = 1.5$) were added to the synthetic scene according to the dichromatic model. To test robustness, we added noise to the foggy images. The noise was randomly selected from a uniformly distributed color cube of dimension 10. The resulting two foggy (and noisy) images are shown in figure 5(b). The structure shown in 5(c) is recovered from the two foggy images using the technique we described above.

Simulations were repeated for the scene in figure 5(a) for two relative scattering coefficient values (β_1 / β_2), and four

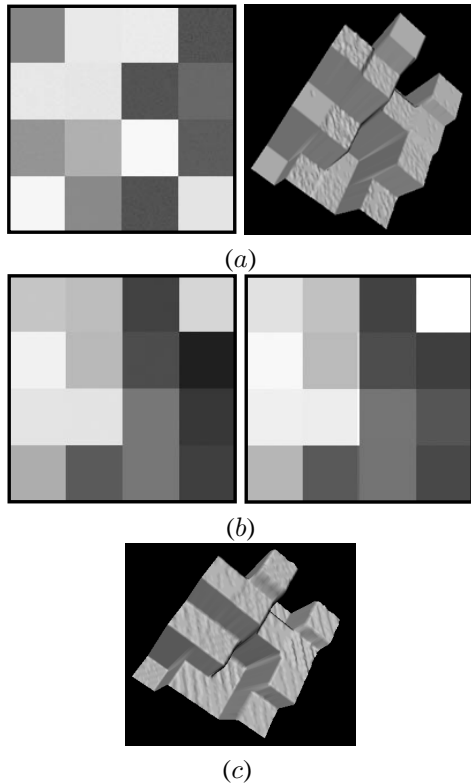


Figure 5: (a) On the left, a 200×200 pixel image representing a synthetic scene with 16 color patches, and on the right, its rotated 3D structure. (b) Two levels of fog ($\beta_1 = 1.0, \beta_2 = 1.5$) are added to the synthetic image according to the dichromatic model. To test robustness, noise is added by random selection from a uniformly distributed color cube of dimension 10. (c) The recovered structure (3×3 median filtered). Refer to [Web00] for version with color images.

| Noise (η) | 0 | 5 | 10 | 15 |
|--------------------------|-----|-------|-------|-------|
| Estimated E_{∞_1} | 100 | 108.7 | 109.2 | 119.0 |
| Estimated E_{∞_2} | 255 | 262.7 | 263.6 | 274.0 |
| Depth Error (%) | 0.0 | 7.14 | 11.7 | 15.3 |

Actual Values $\{\beta_1/\beta_2, E_{\infty_1}, E_{\infty_2}\} = \{0.5, 100, 255\}$

| Noise (η) | 0 | 5 | 10 | 15 |
|--------------------------|-----|-------|-------|-------|
| Estimated E_{∞_1} | 200 | 204.3 | 223.7 | 249.5 |
| Estimated E_{∞_2} | 400 | 403.8 | 417.5 | 444.2 |
| Depth Error (%) | 0.0 | 12.3 | 15.3 | 17.8 |

Actual Values $\{\beta_1/\beta_2, E_{\infty_1}, E_{\infty_2}\} = \{0.67, 200, 400\}$

(b)

Table 2: Simulations were repeated for the scene in figure 5(a), for two sets of parameter values (shown in (a) and (b)), and four different noise levels. Noise was randomly selected from a uniformly distributed color cube of dimension η .

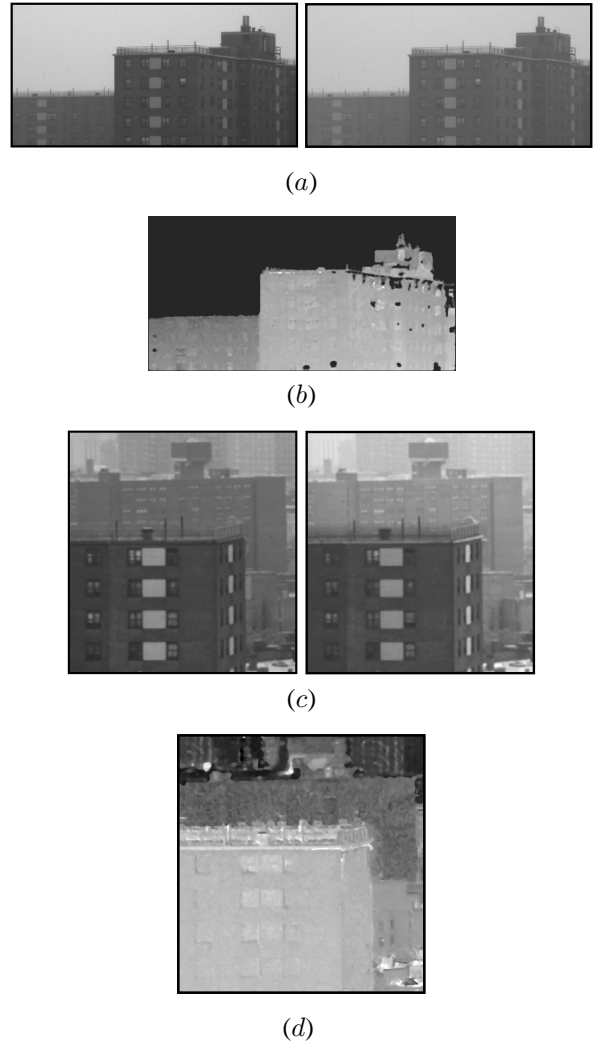


Figure 6: (a) A scene imaged under two different foggy conditions. (b) Computed depth map of the scene using the two images in (a). (c) Another scene imaged under two different hazy conditions. (d) Computed depth map of the scene using the two images in (c). See [Web00] for version with color images.

different noise levels. Once again, the noise was randomly selected from a uniformly distributed color cube of dimension η . Table 2(a) shows results of simulations for the parameter set $\{\beta_1/\beta_2, E_{\infty_1}, E_{\infty_2}\} = \{0.5, 100, 255\}$, while 2(b) shows the results for the set $\{0.67, 200, 400\}$. The computed values for E_{∞_1} , E_{∞_2} , and the percentage RMS error in the recovered scaled depths, computed over all 200×200 pixels are given. These results show that our method for recovering structure is robust for reasonable amounts of noise.

Experiments with two real scenes under foggy and hazy conditions are shown in figure 6. These experiments are based on images acquired using a Nikon N90s SLR camera and a Nikon LS-2000 slide scanner. All images are linearized using the radiometric response curve of the imaging system

that is computed off-line using a color chart. The first of the two scenes was imaged under two foggy conditions, and is shown in 6(a). The second scene was imaged under two hazy conditions as shown in 6(c). Figures 6(b) and 6(d) show the corresponding recovered depth maps.

7 True Scene Color

As we stated in the beginning of the paper, most outdoor vision applications perform well only under clear weather. Any discernible amount of scattering due to fog or haze in the atmosphere, hinders a clear view of the scene. In this section, we compute the direct transmission or “true” colors of the entire scene using minimal *a priori* scene information. For this, we show that, given additional scene information (airlight or direct transmission vector) at a *single* point in the scene, we can compute the true colors of the *entire* scene from two bad weather images.

Consider the dichromatic model given in (8). The observed color of a scene point P_i under weather condition β is,

$$\mathbf{E}^{(i)} = p^{(i)} \hat{\mathbf{D}}^{(i)} + q^{(i)} \hat{\mathbf{A}}, \quad (25)$$

where $p^{(i)}$ is the direct transmission magnitude, and $q^{(i)}$ is the airlight magnitude of P_i . Suppose that the direction $\hat{\mathbf{D}}^{(i)}$ of direct transmission color for a *single* point P_i is given. Besides, the direction $\hat{\mathbf{A}}$ of airlight color for the entire scene can be estimated using (13). Therefore, the coefficients $p^{(i)}$ and $q^{(i)}$ can be computed using (25). Furthermore, the optical thickness βd_i of P_i can be computed from (10).

Since we have already shown how to compute the scaled depth of every scene point (see (20)), the relative depth d_j / d_i of any other scene point P_j with respect to P_i can be computed using the ratio of scaled depths. Hence, the optical thickness and airlight for the scene point P_j , under the *same* atmospheric condition are given by

$$\begin{aligned} \beta d_j &= \beta d_i (d_j / d_i), \\ q^{(j)} &= E_\infty (1 - e^{-\beta d_j}). \end{aligned} \quad (26)$$

Finally, the direct transmission color vector of P_j can be computed as $p^{(j)} \hat{\mathbf{D}}^{(j)} = \mathbf{E}^{(j)} - q^{(j)} \hat{\mathbf{A}}$. Thus, given a *single* measurement (in this case, the direction of direct transmission color of a single scene point), we have shown that the direct transmission and airlight color vectors of any other point, and hence the entire scene can be computed. But how do we specify the true color of any scene point without actually capturing the clear day image?

For this, we assume that there exists atleast one scene point whose true color \mathbf{D} lies *on* the surface of the color cube and we wish to identify such point(s) in the scene. Consider the R-G-B color cube in figure (7). If the true color of a scene point lies *on* the surface of the color cube, then the computed \tilde{q} is equal to the airlight magnitude q of that point.

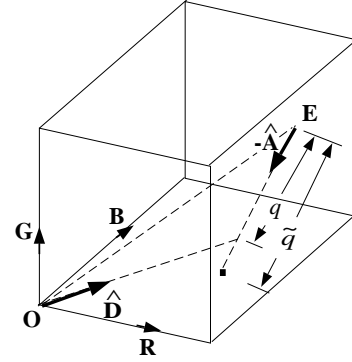


Figure 7: The observed color \mathbf{E} of a scene point, its airlight direction $\hat{\mathbf{A}}$ and true color direction $\hat{\mathbf{D}}$ are shown in the R-G-B color cube. \tilde{q} is the distance from \mathbf{E} to a surface of the cube along negative $\hat{\mathbf{A}}$. For scene points whose true colors do not lie on the cube surface, \tilde{q} is greater than the true airlight magnitude q .



Figure 8: True color images recovered using the two foggy and hazy images shown in figure 6(a) and (c) respectively. The colors in the dark window interiors are dominated by airlight and thus their true colors are black. The images are brightened for display purposes. See [Web00] for the version with color images.

However, if the true color of the point lies *within* the color cube, then clearly $\tilde{q} > q$. For each point P_i , we compute $\tilde{q}^{(i)}$ and optical thickness $\tilde{\beta}_1 d_i$. Note that $\tilde{\beta}_1 d_i$ may or may not be the correct optical thickness. We normalize the optical thicknesses of the scene points by their scaled depths to get

$$\tilde{\alpha}_i = \frac{\tilde{\beta}_1 d_i}{(\beta_2 - \beta_1) d_i}. \quad (27)$$

For scene points that do not lie on the color cube surface, $\tilde{\alpha}_i$ is greater than what it should be. Since we have assumed that there exists atleast one scene point whose true color is on the surface of the cube, it must be the point that has the minimum $\tilde{\alpha}_i$. So, $\tilde{q}^{(i)}$ of that point is its true airlight. Hence, from (26), the airlights and true colors of the entire scene can be computed without using a clear day image.

Usually in urban scenes, window interiors have very little color of their own. Their intensities are solely due to airlight and not due to direct transmission. In other words, their true color is black (the origin of the color cube). We detected such points in the scene using the above technique and recovered the true colors of two foggy and hazy scenes (see figure (8)).

8 Conclusion

In this paper, we presented a general chromatic framework for scene understanding under bad weather conditions. Note that conventional image enhancement techniques are not useful here since the effects of weather must be modeled using atmospheric scattering principles that are closely tied to scene depth. We based our work on the simple yet useful dichromatic model. Several useful constraints on scene color changes due to different atmospheric conditions were derived. Using these constraints, we developed simple algorithms to recover the three dimensional structure and true colors of scenes, from images taken under poor weather conditions. These algorithms were demonstrated for both synthetic and real scenes.

References

- [All76] E. Allard. *Memoire sur l'intensite' et la portee des phares.* paris, dunod. 1876.
- [Bou30] P. Bouguer. *Traite' d'optique sur la gradation de la lumiere.* 1730.
- [CK97] F. Cozman and E. Krotkov. Depth from scattering. *Proceedings of the 1997 Conference on Computer Vision and Pattern Recognition*, 31:801–806, 1997.
- [GC66] J. Gordon and P. Church. Overcast sky luminances and directional luminous reflectances of objects and backgrounds under overcast skies. *Applied Optics*, 5:919, 1966.
- [Hor86] B.K.P. Horn. *Robot Vision.* The MIT Press, 1986.
- [Hul57] Van De Hulst. *Light Scattering by small Particles.* John Wiley and Sons, 1957.
- [Kos24] H. Koschmieder. Theorie der horizontalen sichtweite. *Beitr. Phys. freien Atm.*, 12:33–53,171–181, 1924.
- [McC75] E.J. McCartney. *Optics of the Atmosphere: Scattering by molecules and particles.* John Wiley and Sons, 1975.
- [Mid52] W.E.K. Middleton. *Vision through the Atmosphere.* University of Toronto Press, 1952.
- [MS42] P. Moon and D.E. Spencer. Illumination from a non-uniform sky. *Illum Eng.*, 37:707–726, 1942.
- [NN99] S.K. Nayar and S.G. Narasimhan. Vision in bad weather. *Proceedings of the 7th International Conference on Computer Vision*, 1999.
- [Web00] Website. http://www.cs.columbia.edu/cave/research/publications/vision_weather.html. 2000.

A Direct Transmission under Overcast Skies

We present an analysis of the effect of sky illumination and its reflection by a scene point, on the direct transmission from the scene point. For this, we make two simplifying assumptions on the illumination received by scene points. Usually, the sky is overcast under foggy conditions. So we use the overcast sky model[GC66] for environmental illumination. We also assume that the irradiance of each scene

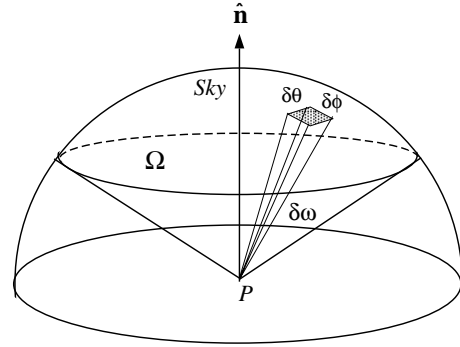


Figure 9: The illumination geometry of a scene point P with surface normal $\hat{\mathbf{n}}$. The irradiance of P is due to the airlight radiance of its sky aperture Ω .

point is dominated by the radiance of the sky, and that the irradiance due to other scene points is not significant.

Consider the illumination geometry shown in figure (9). Let P be a point on a surface and $\hat{\mathbf{n}}$ be its normal. We define the *sky aperture* Ω of point P , as the cone of sky visible from P . Consider an infinitesimal patch of the sky, of size $\delta\theta$ in polar angle and $\delta\phi$ in azimuth as shown in figure (9). Let this patch subtend a solid angle $\delta\omega$ at P . For overcast skies, Moon[MS42] and Gordon[GC66] have shown that the radiance of the infinitesimal cone $\delta\Omega$, in the direction (θ, ϕ) is given by $L(\theta, \phi) = L_\infty(\lambda)(1 + 2\cos\theta)\delta\omega$, where $\delta\omega = \sin\theta \delta\theta \delta\phi$. Hence, the irradiance at P due to the entire aperture Ω , is given by

$$E(\lambda) = \int \int_{\Omega} L_\infty(\lambda) (1 + 2\cos\theta) \cos\theta \sin\theta d\theta d\phi, \quad (28)$$

where $\cos\theta$ accounts for foreshortening [Hor86]. If R is the BRDF of P , then the radiance from P toward the observer can be written as

$$L_0(\lambda) = \int \int_{\Omega} L_\infty(\lambda) f(\theta) R(\theta, \phi) d\theta d\phi, \quad (29)$$

where $f(\theta) = (1 + 2\cos\theta) \cos\theta \sin\theta$. Let σ be the projection of a unit patch around P , on a plane perpendicular to the viewing direction. Then, the radiant intensity of P is given by $I_0(\lambda) = \sigma L_0(\lambda)$. Since $L_\infty(\lambda)$ is a constant with respect to θ and ϕ , we can factor it out of the integral and write concisely as $I_0(\lambda) = L_\infty(\lambda) r$, where $r = \sigma \int \int_{\Omega} f(\theta) R(\theta, \phi) d\theta d\phi$. This term r represents the sky aperture and the reflectance in the direction of the viewer. Substituting for $I_0(\lambda)$ in the direct transmission model in (5), we obtain

$$E(d, \lambda) = g \frac{L_\infty(\lambda) r e^{-\beta(\lambda)d}}{d^2}. \quad (30)$$

We have thus formulated the direct transmission model in terms of overcast sky illumination and the reflectance of the scene points.